Dielectric technique to measure the twist elastic constant of liquid crystals: The case of a bent-core material

P. Salamon and N. Éber
Institute for Solid State Physics and Optics, Wigner Research Centre for Physics, Hungarian Academy of Sciences, H-1525 Budapest, P.O.B. 49, Hungary

J. Seltmann
Institute of Chemistry, Chemnitz University of Technology, Strasse der Nationen 62, 09111 Chemnitz, Germany

M. Lehmann
Institute of Organic Chemistry, University of Würzburg, Am Hubland, 97074 Würzburg, Germany

J. T. Gleeson and S. Sprunt
Department of Physics, Kent State University, Kent, Ohio 44242, USA

A. Jákli
Liquid Crystal Institute, Kent State University, Kent, Ohio 44242, USA
(Received 21 February 2012; published 14 June 2012)

The effect of director pretilt on the twist magnetic Fréedericksz transition of nematics was investigated in a planar cell. The director configuration was calculated as a function of magnetic inductance. The dielectric and optical response of the nematic liquid crystal was numerically modeled. A dielectric measurement method for determining the elastic constant K_{22} is presented. The influence of the conditions for the Mauguin effect is discussed. The theoretical predictions were confirmed by our experiments. Experimental data for all elastic constants of a bent-core nematic material are presented and discussed.

DOI: 10.1103/PhysRevE.85.061704 PACS number(s): 77.84.Nh, 78.15.+e, 61.30.−v

I. INTRODUCTION

The precise knowledge of material parameters is always valuable information for both applied and basic research. It helps to further improve or develop devices for industrial or scientific purposes and serves as input data for each and every phenomenon to understand, while the anomalous behavior of the parameters can refer to a novel effect or can be itself a phenomenon to understand.

Elasticity is one of the most common characteristics of liquid crystals. In nematic liquid crystals, there are three independent types of director deformation (splay, twist, bend) with the corresponding elastic constants K_{11}, K_{22}, K_{33}, respectively [1]. Naturally, most liquid crystalline phenomena are strongly affected by elasticity. However, only a few effects are in practice used to measure the elastic constants due to precision issues.

The determination of K_{11} and of K_{33} is relatively simple by studying Fréedericksz transitions induced by electric and magnetic fields in different geometries [1–3]. With the help of numerical simulation and fitting methods, several material parameters (including K_{11}, K_{33}, and the diamagnetic anisotropy χ_a) can be easily obtained from optical transmittance and by dielectric measurements in applied magnetic and electric fields, in the so-called splay geometry using a single planar cell [3].

Determining K_{22} in a similar way in the so-called twist-Fréedericksz geometry using a planar cell is much less trivial due to the problems discussed below, thus there were different other techniques employed. There were attempts to determine the Fréedericksz threshold by measuring birefringence in a planar cell using obliquely incident light [4,5] or applying electric and/or magnetic fields on a twisted nematic cell [6–8]. Other optical methods were also developed including conoscopic techniques [9–11], half leaky guided wave measurements [12], and methods based on light scattering [13–19]. Other techniques used cells with special in-plane electrodes [20–24]. Further experiments were carried out on wedge [25,26] and π cells [27]. K_{22} could also be determined in a torsion pendulum experiment in magnetic field [28].

In the twist-Fréedericksz geometry, the problems mentioned above affect both the optical transmittance and dielectric techniques. Due to the Mauguin effect, the polarization of the light follows the director and passes the cell almost unaffected under certain conditions [1,2]. The deformation thus can be detected only by measuring the depolarization occurring due to the failure of that conditions. In the present paper, we study these conditions for the Mauguin effect with a simulation technique, and we present our suggestions on how to overcome this problem during measurements.

Considering an ideal planar cell with indium tin oxide (ITO) electrodes on the glass substrates, no change in the capacitance due to twist deformation is expected. It will be shown, however, that this latter anticipation is not true in the presence of pretilt. We present a dielectric technique to measure K_{22} in a standard planar cell, which is, in several aspects, more versatile than the optical methods. We note that our technique differs from the dielectric method published in Ref. [20], which requires specially designed cells for the measurements.

Bent-core liquid crystals (BCs) are the subject of numerous studies currently, because of their fascinating features. The

reduced molecular symmetry of BCs compared to that of rodlike materials gave rise to many discoveries. Nonconventional, so-called banana phases were found ($B_1, B_2, \ldots, B_8$) with unique properties (e.g., macroscopic chirality formed by achiral molecules [29]). Bent-core nematics (BCNs) are also in the focus of the research interest. Dielectric properties [30], flexoelectricity [31,32], pattern formation [33–37], and the presence of smectic clusters or cybotactic groups [38–40] are widely studied areas in BCNs. Anomalous elasticity of BCNs was published recently by several groups [3,41–43]. There seem to be general tendencies in the magnitudes and ratios of elastic constants in the case of BCNs. The magnitudes of K_{22} and K_{33} were found to be unusually small compared to rodlike nematics. The small $K_{22} : K_{11}$ and $K_{33} : K_{11}$ ratios were attributed to the presence of possibly chiral smectic clusters and the favorable bend distortion originating in the bent shape of the molecules.

In this paper we report about studies on the magnetic Fréedericksz transition in the presence of a director pretilt, and present the measurements of all Frank elastic constants of a BCN compound, where K_{22} was determined using the dielectric measurement technique described below.

The paper is organized as follows. In Sec. II the details of the theoretical description of the twist-Fréedericksz transition can be found. In Sec. III the results of our numerical calculations are shown and discussed. In Sec. IV our experimental technique is introduced. In Sec. V the results of the elastic constant measurements on a bent-core material are presented and compared with our calculations. Finally, in Sec. VI we summarize the results obtained.

II. THEORETICAL CONSIDERATIONS

A nonzero angle between the director and the alignment layer at the surface is called the pretilt. We consider a planar cell with strong anchoring and a pretilt of Θ_0, filled with a nematic liquid crystal with positive diamagnetic anisotropy ($\chi_a > 0$). To achieve an undistorted initial director profile, the pretilt angles should be the same at the two bordering surfaces. This condition is a realistic assumption for the description of a cell with alignment layers rubbed antiparallelly. The geometry of the system can be seen in Figs. 1(a)–1(b). The film thickness is denoted by d. The initial undistorted director field is perpendicular to the y direction. Homogenous magnetic inductance $\mathbf{B} = (B_x, B_y, B_z)$ is applied in a general direction. The magnitude of the field is denoted by $B = |\mathbf{B}|$. The pure twist geometry, however, corresponds to $B_x = B_z = 0$. For simplicity we will use this case unless it is noted otherwise. Nevertheless our model can handle magnetic fields lying along a general direction. We will utilize this later when describing the case where $\mathbf{B}$ is slightly tilted from the y direction. In that way our model is more realistic to explain the effect of improperly adjusted geometry in the experiments.

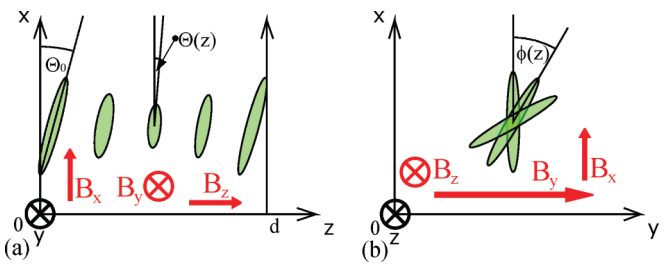

FIG. 1. (Color online) Two views on the twist-Fréedericksz geometry with pretilt. (a) cross section normal to the substrates, (b) view parallel to the substrates.

With no pretilt, a magnetic inductance exceeding the threshold value B_{th} induces the twist-Fréedericksz transition, where the director profile can be described with one variable: the twist angle ϕ. In the presence of a director pretilt, a second variable, the tilt angle Θ is also necessary for a complete description of the director field. The director components expressed by the two angles are

$$\mathbf{n} = (\cos\Theta\cos\phi, \cos\Theta\sin\phi, \sin\Theta). \tag{1}$$

The torques acting on the director in a magnetic field lead to a change of both ϕ and Θ. The deformation is homogenous, both angles depend only on the z coordinate. We assume that the cell is symmetric, therefore the maximum deformation occurs in the midplane (at $z = d/2$).

The total free energy density is the sum of the elastic and of the magnetic components:

$$f_{\text{free}} = f_{\text{el}} + f_{\text{magn}}, \tag{2}$$

$$f_{el} = \frac{1}{2}K_{11}(\nabla\mathbf{n})^2 + \frac{1}{2}K_{22}[\mathbf{n}(\nabla\times\mathbf{n})]^2 + \frac{1}{2}K_{33}[\mathbf{n}\times(\nabla\times\mathbf{n})]^2, \tag{3}$$

$$f_{\text{magn}} = -\frac{1}{2}\frac{\chi_a}{\mu_0}(\mathbf{nB})^2. \tag{4}$$

Plugging in the director profile of Eq. (1), we get

$$\begin{aligned} f_{\text{free}} = {} & \frac{1}{2}f(\Theta)\Theta'^2 + \frac{1}{2}g(\Theta)\phi'^2 - \frac{1}{2}\frac{\chi_a}{\mu_0}\big[B_x^2\cos^2\Theta\cos^2\phi \\ & + B_y^2\cos^2\Theta\sin^2\phi + B_z^2\sin^2\Theta \\ & + 2B_xB_y\cos^2\Theta\sin\phi\cos\phi \\ & + 2B_xB_z\sin\Theta\cos\Theta\cos\phi \\ & + 2B_yB_z\sin\Theta\cos\Theta\sin\phi\big], \end{aligned} \tag{5}$$

where prime refers to derivation with respect to z and

$$f(\Theta) = K_{11}\cos^2\Theta + K_{33}\sin^2\Theta, \tag{6}$$

$$g(\Theta) = \cos^2\Theta(K_{22}\cos^2\Theta + K_{33}\sin^2\Theta). \tag{7}$$

We use Euler-Lagrange equations to minimize the free energy to obtain the equilibrium solutions for $\Theta(z)$ and for $\phi(z)$:

$$\frac{d}{dz}\left(\frac{\partial f_{\text{free}}}{\partial\Theta'}\right) - \frac{\partial f_{\text{free}}}{\partial\Theta} = 0, \tag{8}$$

$$\frac{d}{dz}\left(\frac{\partial f_{\text{free}}}{\partial\phi'}\right) - \frac{\partial f_{\text{free}}}{\partial\phi} = 0. \tag{9}$$

After combining Eqs. (6)–(9), one arrives to a set of two second-order coupled nonlinear ordinary differential equations. This is a boundary value problem, with the mixed boundary conditions: $\Theta(0) = \Theta_0$, $\phi(0) = 0$, $\Theta'(d/2) = 0$, and $\phi'(d/2) = 0$. The numerical solution of the equations was provided by a MATLAB program.

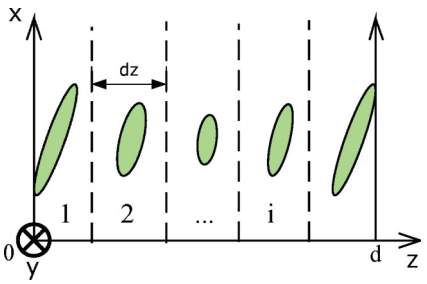

FIG. 2. (Color online) The planar cell that is split into thin slabs for optical calculations.

The changes in the director field are usually monitored by dielectric or optical techniques. A later comparison with experiments thus requires the calculation of the cell capacitance and its optical transmittance. As the cell is inhomogeneous in the z direction, it is first split into thin slabs of thickness dz as shown in Fig. 2. The cell capacitance C is the net of the capacitances of all slabs connected in series. In the $dz \to 0$ limit one obtains

$$C = C_0 \varepsilon_{\text{eff}} = C_0 d \left(\int_0^d \frac{1}{\varepsilon_\perp + \varepsilon_a \sin^2 \Theta(z)} dz \right)^{-1}, \quad (10)$$

where C_0 is the capacitance of the empty cell, ε_{eff} is an effective, $\varepsilon_\perp$ is the perpendicular dielectric constant, and ε_a is the dielectric anisotropy.

The optical response of the cell has been calculated with the Mueller-matrix method [44–46]. A (partially) polarized light can be described by a four-element Stokes vector. Its definition and an example of a Stokes vector for light linearly polarized in the x direction can be found in the Appendix. The effect of an optical element on the incoming light is characterized by a specific Mueller matrix. The light transmittance then can be calculated by matrix multiplication.

To calculate the Mueller matrix of the cell, we split it into thin slabs of thickness dz as described above. If dz is small enough, the twist and tilt angles can be regarded constant in a slab with a good approximation. Each slab is then a birefringent wave plate with a phase shift $\Delta\varphi_i$ and the direction of its slow axis making an angle ϕ_i with the x axis. The phase difference for the ith slab coming from its birefringence can be calculated as

$$\Delta\varphi_i = \frac{2\pi}{\lambda} \left(\frac{n_e}{\sqrt{1 + \frac{n_e^2 - n_o^2}{n_o^2} \sin^2 \Theta_i}} - n_o \right) dz, \quad (11)$$

where λ is the wavelength of light, n_o and n_e are the ordinary and extraordinary refractive indices of the liquid crystal, respectively, while Θ_i is the tilt angle at the position of the ith slab. The Mueller matrix of the ith slab of our liquid crystal cell is $\mathbf{M}_{wp}(\phi_i, \Delta\varphi_i)$. We also introduce $\mathbf{M}_{\text{pol}}(\alpha)$, the Mueller matrix of a polarizer placed at an angle α with respect to the x direction in our geometry. The matrices can be found in the Appendix. The liquid crystal cell is placed between polarizers. The angles of the polarizer and analyzer are α_p and α_a, respectively. If the cell is illuminated with an incident monochromatic light with a Stokes vector of $\mathbf{s}_{\text{in}}$, the Stokes-vector of the outgoing light, $\mathbf{s}_{\text{out}}$, can be calculated as

$$\mathbf{s}_{\text{out}} = \mathbf{M}_{\text{pol}}(\alpha_a) \left(\prod_{i=1}^{n} \mathbf{M}_{wp}(\phi_i, \Delta\varphi_i) \right) \mathbf{M}_{\text{pol}}(\alpha_p) \mathbf{s}_{\text{in}}. \quad (12)$$

The optical transmittance is given by the ratio of the first elements of $\mathbf{s}_{\text{out}}$ and of $\mathbf{s}_{\text{in}}$. $\mathbf{s}_{\text{in}}$ was chosen to be linearly polarized in the direction of α_p (parallel to the polarizer).

We set $\alpha_p = 0$ and $\alpha_a = 90^\circ$, thus the optical transmittance is proportional to the expected depolarization.

III. SIMULATION RESULTS AND DISCUSSION

During simulations the magnetic inductance values were counted in units of $B_{\text{th}} = \frac{\pi}{d} \sqrt{\frac{\mu_0 K_{22}}{|\chi_a|}}$, which is the Fréedericksz threshold inductance for the twist geometry with zero pretilt. All the simulations were performed using the material parameters of **5CB** [3]. A pretilt of $\Theta_0 = 2^\circ$ was assumed. Figures 3(a)–3(b) show the change in the calculated twist and tilt angles inside the sample for three different magnetic inductances. Below the threshold, at $B/B_{\text{th}} = 0.5$, there is no deformation, ϕ remains zero while $\Theta(z) = \Theta_0$. Above the threshold the twist angle increases, while the tilt angle decreases, just as it was expected. At higher inductances, ϕ approaches 90°, while Θ goes to 0 far from the substrates.

We define β as a small misalignment angle of $\mathbf{B}$ from the y direction in the y-z plane, thus $\tan\beta = B_z/B_y$ (and $B_x = 0$). We have calculated the effective permittivity (ε_{eff}) defined in Eq. (10) for $0 < B < 5B_{\text{th}}$ in two cases: the first is the

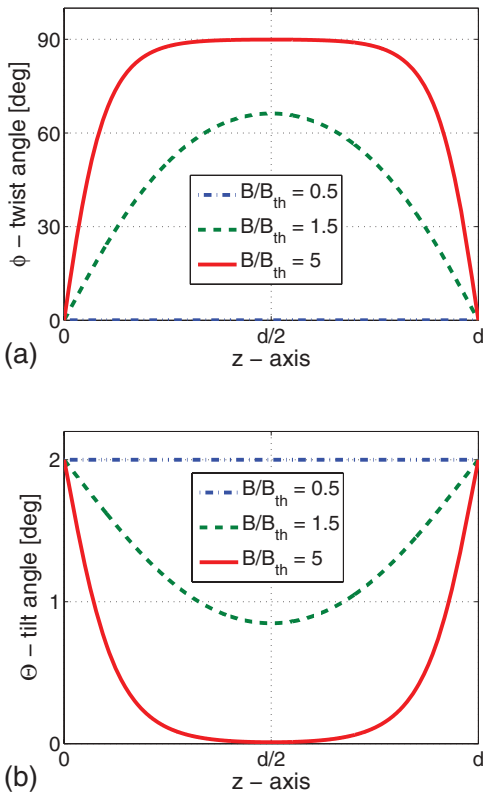

FIG. 3. (Color online) The simulated director configuration at different applied magnetic inductances described by the ϕ twist angle (a) and the Θ tilt angle (b) shown along the z direction of the cell.

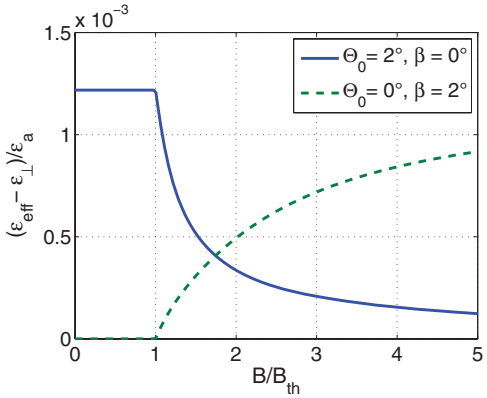

FIG. 4. (Color online) The calculated reduced dielectric constant as the function of relative magnetic inductance during the twist-magnetic-Fréedericksz transition. Solid line: untilted field and director pretilt of $\Theta_0 = 2^\circ$; dashed line: tilted field and no pretilt.

perfectly aligned geometry with pretilt ($\Theta_0 = 2^\circ$ and $\beta = 0^\circ$), the other is a misaligned case with no pretilt ($\Theta_0 = 0^\circ$ and $\beta = 2^\circ$). As $\varepsilon_\perp < \varepsilon_{\text{eff}} < \varepsilon_{||}$ always fulfils for liquid crystal samples with $\varepsilon_a > 0$, for the visualization of the magnetic field dependence of ε_{eff} it is convenient to plot the reduced quantity $(\varepsilon_{\text{eff}} - \varepsilon_\perp)/\varepsilon_a$, as presented in Fig. 4 (solid and dashed lines for the two cases correspondingly).

It is important to emphasize at this point that without a director pretilt ($\Theta_0 = 0^\circ$) in a perfectly aligned geometry ($\beta = 0^\circ$) no change is expected in ε_{eff} as it does not depend on ϕ. If we have $\Theta_0 \neq 0$ in Fig. 4, however, a Fréedericksz transition with sharp threshold behavior can clearly be seen. The sharp transition is owing to the fact that the initial director is perpendicular to **B** even in the presence of a pretilt, in contrast to the splay geometry (see Fig. 10), where the pretilt makes the threshold smooth. This effect thus gives us a dielectric measurement technique to study the twist-Fréedericksz transition and use it to determine K_{22}. This technique could be widely applied, because a small, well defined pretilt is always present as a consequence of the rubbing of a planar polyimide alignment layer. The threshold inductance value is seemingly very close to B_{th} defined before, which can be expected for the case of a small pretilt. Below the threshold $\varepsilon_{\text{eff}} = \varepsilon_\perp + \varepsilon_a \sin^2 \Theta_0$, while towards high inductances it converges to $\varepsilon_\perp$. The maximum change of ε_{eff} is thus in the order of 0.1% of ε_a for usual pretilts. This is a small value, especially for compounds with low dielectric anisotropy, however, a good capacitance bridge has a resolution in the order of parts per million (or better), so is more than capable of performing such measurement.

A change of Θ also occurs at no pretilt if the magnetic field has a small misalignment (Fig. 4, dashed line). Here the magnetic field is also perpendicular to the initial director, thus we can see a sharp transition. The change in the effective dielectric constant here is due to the presence of $B_z \neq 0$ and is of the same order of magnitude as in the pretilt case. The relative change has, however, an opposite sign. In the more realistic case where both $\Theta_0 \neq 0$ and $\beta \neq 0$, the two effects counteract together reducing the change in ε_{eff}. Furthermore the transition is expected to be less sharp, because **B** is then not perpendicular to the initial director. As a consequence, misalignment of the field should be avoided in an experiment in order to obtain precise data. This can be achieved by using a sample holder with appropriate geometrical constraints with respect to the poles of the magnet.

Calculation of the director field also allows the study of the optical behavior of the cell. It is well known that the adiabatic light propagation along a cholesteric helix requires the Mauguin condition, $\lambda \ll P n_a$ to satisfy (P is the helical pitch, and $n_a = n_e - n_o$ is the optical anisotropy) [1]. In our twist-Fréedericksz geometry the gradient of the twist angle, ϕ', plays the role of the wave number of the helix, thus the above condition is the equivalent of $\lambda \ll \frac{2\pi}{\phi'} n_a$. It is convenient to introduce a dimensionless quantity, $\eta = \frac{2\pi}{\lambda \max(\phi')} n_a$ as a measure of how well the Mauguin condition ($1 \ll \eta$) fulfills [$\max(\phi')$ is the maximal value of $\phi'(z)$ in the cell]. As η decreases, one gradually leaves the adiabatic light propagation regime, thus the depolarization of the transmitted light becomes stronger. Though this is a continuous transition, for a qualitative analysis of the dependence on magnetic inductance, pretilt angle and cell thickness it is convenient to choose an arbitrary large number (e.g., $\eta_c = 20$) as a discriminating value. Then one can (approximately) say that being in the Mauguin limit corresponds to $\eta > \eta_c$.

In our geometry the twist is induced by the magnetic inductance. Figure 5 shows η versus B/B_{th} calculated for a $d = 30\,\mu$m thick cell assuming different pretilt angles. The monotonic decrease of $\eta(B/B_{\text{th}})$ means that the higher the magnetic inductance above B_{th}, the less adiabatic the light propagation through the cell. This is due to the increasing ϕ gradients near the substrates as seen also in Fig. 3(a). One can formally introduce a critical magnetic inductance B_c with $\eta(B_c) = \eta_c$. For $B/B_{\text{th}} > B_c$ one is outside the Mauguin limit, therefore strong depolarization is expected. For $B/B_{\text{th}} < B_c$, however, light propagates adiabatically, therefore depolarization is small; the measurement of depolarization might not be sensitive enough for studying the Fréedericksz transition.

Figure 5 shows that the $\eta(B/B_{\text{th}})$ curves and thus B_c shifts toward higher B/B_{th} values if a director pretilt is introduced (i.e., the pretilt reduces the ϕ gradients).

Figure 6 exhibits the thickness dependence of B_c. It is seen that the growth of B_c with d is substantial. This implies that the proper choice of the cell thickness is really

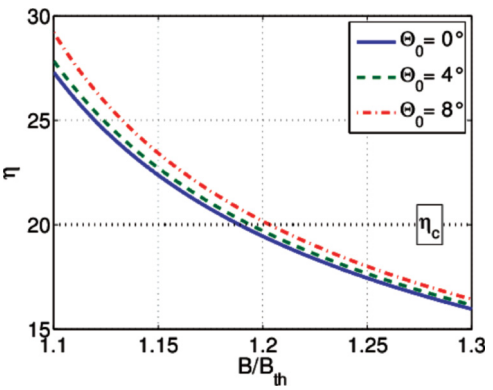

FIG. 5. (Color online) The η as a function of the magnetic inductance calculated for three pretilt values. ($d = 30\,\mu$m).

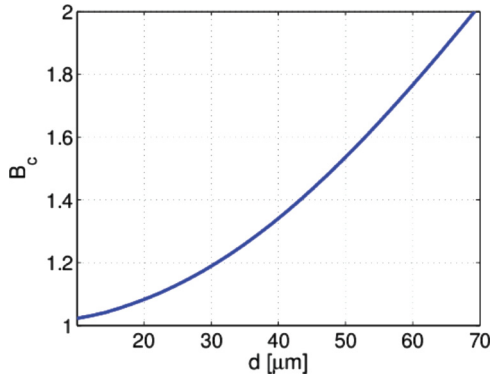

FIG. 6. (Color online) The thickness dependence of B_c.

important for studying the twist-Fréedericksz transition by optical depolarization measurements; low thickness with low pretilt gives the best results. We should emphasize, however, again that η_c and B_c are not real thresholds, but just helpful tools to obtain the conclusions above purely from knowing the director field in the cell.

Calculation of the actual optical transmittance confirmed the tendencies concluded in the previous paragraph. Figure 7 depicts the magnetic inductance dependence of the transmittance in cells of different thicknesses, but without pretilt, under the conditions of crossed polarizers, with the polarizer parallel with the initial director.

It is evident that the transition is much sharper and the transmittance is much larger in a thinner cell. We can conclude that the optical measurement problems described in Ref. [2] are actually present only for thicker cells; the technique works well for thin cells, though there higher magnetic inductances are needed. Nevertheless, moderate $B \sim 1$ T inductances may be sufficient (e.g., for a 10 μm thick planar cell filled with **5CB**: $B_{\text{th}} = 0.6$ T).

When a director pretilt is present, both the twist and the tilt angles change with the applied field. Consequently the transmitted light intensity depends, besides the depolarization, on the birefringence variation too. This is demonstrated in Fig. 8, which presents the calculated transmittance of a $d = 30\,\mu$m cell for three different pretilt values. The main feature of this plot is the appearance of a hump at the highest pretilt,

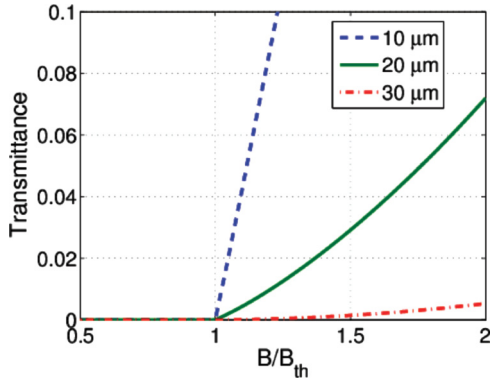

FIG. 7. (Color online) The magnetic inductance dependence of the calculated transmittance for three different cell thickness in the twist-Fréedericksz transition with no pretilt.

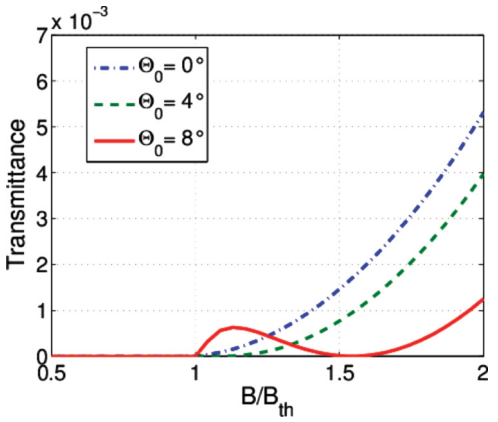

FIG. 8. (Color online) The magnetic inductance dependence of the calculated transmittance for three different pretilt values in the twist-Fréedericksz transition. ($d = 30\,\mu$m)

which we attribute to the effect of birefringence. We note that at higher thickness and pretilt values, the intensity oscillations strongly depend on the parameters of the cell (e.g., thickness, material constants), thus the interpretation of a measurement curve is rather difficult. This is another argument for the use of thin cells.

IV. EXPERIMENTAL TECHNIQUE

In order to demonstrate the usability of the dielectric method to determine K_{22}, we have prepared an experiment on the well known compound 4′-pentyl-4-cyanobiphenyl (5CB). Experiments on a different setup have been carried out on the bent-core material abbreviated as DT6PY6E6 [47] (Thiadiazol with a pyridine arm with two hexyloxy chains and an ester arm with two lateral hexyloxy chains. The ethyl ester is connected via a hexamethylene spacer.). Its chemical structure is shown in Fig. 9.

The synthesis and the molecular properties of the compound have been published recently [47]. DT6PY6E6 has a nematic phase in a relatively wide temperature range. The clearing point is $T_{NI} = 149$ °C, the melting point is at 93 °C in heating, while the nematic phase can be supercooled down to room temperature.

The different custom made sandwich cells with ITO electrodes were filled with 5CB and with DT6PY6E6 in the isotropic phase. The thickness of the empty cells were $d = 26\,\mu$m and $d = 27.3\,\mu$m, respectively. d was measured by interferometry. Rubbed polyimide was used as alignment

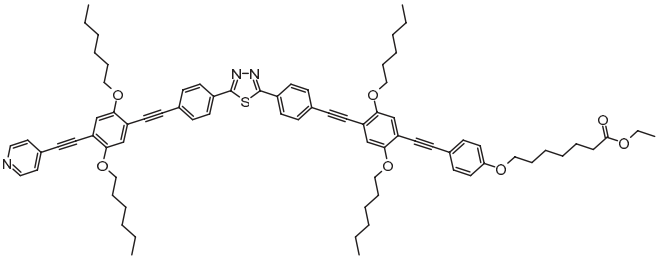

FIG. 9. The chemical structure of the bent-core compound DT6PY6E6.

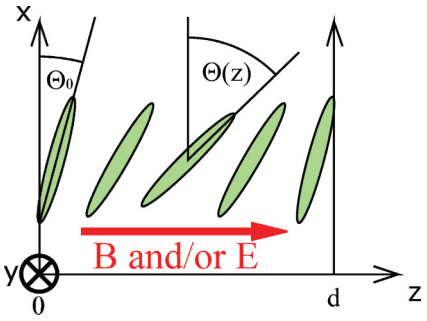

FIG. 10. (Color online) The schematic figure of the splay-Fréedericksz transition geometry.

layers; polarizing microscopy confirmed uniform planar alignment in both cases.

In the case of 5CB, we have determined $\varepsilon_{\rm eff}$ versus B in the twist geometry (Fig. 1). $\varepsilon_{\rm eff}$ was obtained as the ratio of the filled and the empty cell capacitances, which were calculated from the complex impedances of the cell assuming a parallel RC equivalent circuit. The impedances were derived using Ohm's law. Sinusoidal voltage with 30 mV amplitude at 1 kHz frequency was switched to the cell while the current was measured in the circuit with the help of an Ithaco Model 1642 current sensitive preamp. The applied voltage and the signal proportional to the current was measured by the two oscilloscope channels of a TiePie Handyscope HS3 instrument. The impedances of the cables and of the open circuit were measured and the values were used for corrections of the results on the liquid crystal cell. The voltage signal was provided by the function generator output of the same device. The sample was put between the poles of an electromagnet in a temperature stabilized stage.

In the case of DT6PY6E6 we have measured the capacitance and the transmitted intensity (I) between crossed polarizers on a planar liquid crystal cell as a function of B. The effective dielectric constant $\varepsilon_{\rm eff}$ was calculated as the ratio of the filled and the empty cell capacitances. The experiment was carried out in two geometries. The splay geometry is illustrated in Fig. 10; the twist geometry was shown before in Fig. 1. In the splay (twist) geometry, **B** is perpendicular (parallel) to the plane of the substrates. We were also able to measure the voltage dependence of the transmitted intensity during the electric splay-Fréedericksz transition, due to the positive ε_a of the compound. The voltage was provided by the amplified 1 kHz sinusoidal signal of an Agilent 33120A function generator. Our sample was kept in a custom-made temperature controlled heat stage with a temperature stability better than 0.1 °C. The applied magnetic inductance was provided by an electromagnet in the range of $B = 0$–1.3 T. The inductance was measured by a Hall probe. The capacitance of the cell was measured by a high-precision Andeen-Hagerling 2500A capacitance bridge at 1 kHz. We used a 4 mW high-stability He-Ne laser ($\lambda = 633$ nm) as light source and a Thorlabs PDA55 photodetector connected with a digital multimeter to measure the transmitted intensity. We note that in the twist case, we also tried to measure the small intensity signal with lock-in technique using a chopper, however, the results were the same as in the simpler former technique. The sample was put between crossed polarizers. In the splay geometry the polarizer was adjusted to 45° with respect to the initial director to get the highest intensity, while this angle was set to zero in the other case, where only the depolarization had to be measured.

Both measurement systems were automatized and controlled by LABVIEW programs.

V. EXPERIMENTAL RESULTS AND DISCUSSION

The magnetic inductance dependence of $\varepsilon_{\rm eff}$ in the twist geometry for 5CB at $T_{NI} - T = 8$ °C is presented in Fig. 11.

The best numerical fit of the dielectric data is shown by the solid line. (The following material constants used by the fit were taken from the literature: $K_{11} = 5.9$ pN and $K_{33} = 10$ pN [19], $\varepsilon_{||} = 17.5$ [48], and $\chi_a = 1.2 \cdot 10^{-6}$ [49].) From the threshold inductance (see dotted line) we have $K_{22} = 4.2$ pN, which is close to the literature value of $K_{22} = 3.9$ pN [19]. The fit value of the pretilt is $\Theta_0 = 1.5°$, which is realistic. Our data are moderately noisy, but they clearly show that the principle of the measurement is working and the measurements with adequate precision can be realized even with a regular oscilloscope. We have measured a decreasing effective dielectric constant during the transition, which means the change in $\varepsilon_{\rm eff}$ originates dominantly from the presence of a pretilt.

The magnetic inductance dependence of $\varepsilon_{\rm eff}$ and the voltage dependence of the optical phase difference $\Delta\Phi$ in the splay geometry for the compound DT6PY6E6 at $T = 125$ °C are shown in Figs. 12 and 13, respectively.

The solid lines correspond to experimental data recorded with a high sample density. The dashed lines are numerical fits obtained using the numerical methods published in Ref. [3] to extract the material parameters from the experimental data. The quality of the fits are saliently good. We have determined the elastic constants: $K_{11} = 5.4$ pN, $K_{33} = 10$ pN; the diamagnetic anisotropy: $\chi_a = 7.4 \cdot 10^{-7}$; the dielectric constants: $\varepsilon_\perp = 4.1$, $\varepsilon_{||} = 5.9$; and the optical anisotropy: $n_a = 0.24$.

The magnetic inductance dependence of $\varepsilon_{\rm eff}$ and of the transmitted intensity measured in the twist geometry in DT6PY6E6 is presented in Fig. 14 by solid and dash-dotted curves, respectively. The best numerical fit of the dielectric

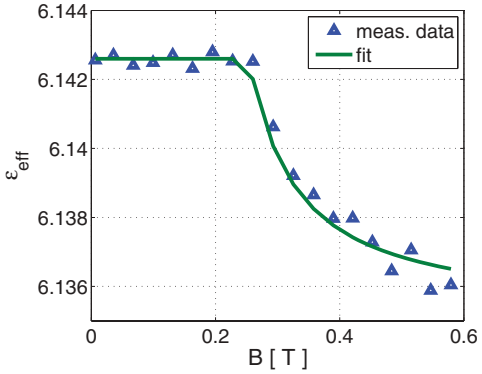

FIG. 11. (Color online) The magnetic inductance dependence of $\varepsilon_{\rm eff}$ in the twist-Fréedericksz transition for the compound 5CB at $T_{NI} - T = 8$ °C. The triangles are experimental data points. The solid line is numerical fit.

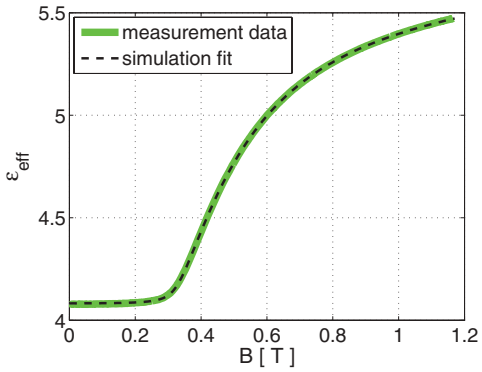

FIG. 12. (Color online) The magnetic inductance dependence of ε_{eff} in the splay-Fréedericksz transition for the compound DT6PY6E6 at $T = 125\,^{\circ}$C. The solid line is experimental data. The dashed line is numerical fit.

data is shown by the dashed line. (The values of K_{33} and of χ_a determined by the fit in the splay geometry were used here.) From the threshold inductance (see dotted line) we have $K_{22} = 2.2$ pN. The optical intensity is more noisy than the dielectric data in spite of the fact that the relative change in the latter is in the order of $1/1000$. It seems to be more difficult to locate the threshold by the optical method. Comparing this measurement with the one prepared on 5CB, here also stands that due to the decrease in ε_{eff}, the effect dominantly originates from the presence of pretilt. This dataset is much less noisy, because the precision of the capacitance bridge is much higher than that of the oscilloscope technique presented above.

The Frank elastic constant values of DT6PY6E6 do not follow the trends reported by independent authors [3,41–43] for bent-core compounds. The elastic constants of DT6PY6E6 can rather be considered as typical for rodlike liquid crystals. K_{22} is rather low, however, it is not as low ($\sim$0.3 pN) as for the BCN in Ref. [3]. The magnitude of K_{33} is large and $K_{33}/K_{11} > 1$.

We think that the non-BCN behavior of DT6PY6E6 might be due to the effect of the four alkyl chains connected to intermediate core rings. The alkyl chains can easily change conformation with relatively low energy cost (they are not rigid). They can act like soft spacers between molecules. Thus,

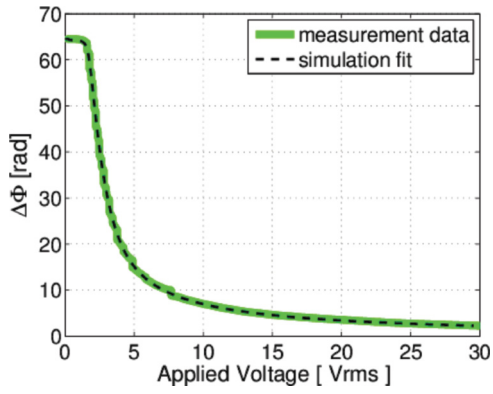

FIG. 13. (Color online) The voltage dependence of $\Delta\Phi$ in the splay-Fréedericksz transition for the compound DT6PY6E6 at $T = 125\,^{\circ}$C. The solid line is experimental data. The dashed line is numerical fit.

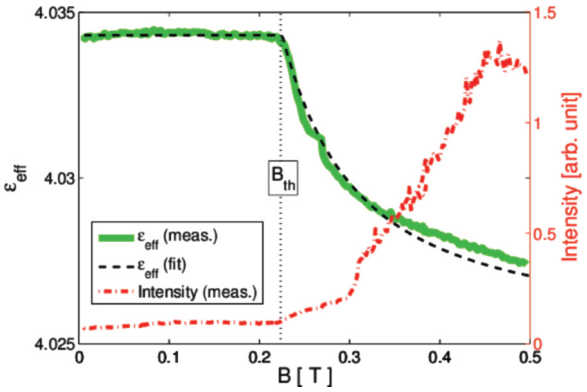

FIG. 14. (Color online) The magnetic inductance dependence of ε_{eff} (measured data: solid line, fit: dashed line) and of the transmitted intensity (dash-dotted line) measured on DT6PY6E6 in the twist geometry. The B_{th} threshold inductance determined by the fit is at the dotted line.

for topological reasons, the chains might prevent the direct steric interaction between the rigid bent shaped cores in the nematic phase. Therefore the system looses its tendency to favor a polar packing, which has led to unusual properties via smectic cluster formation in other BCNs. This idea is in accordance with x-ray results on DT6PY6E6 [47]. The distance between molecules are unusually large, which could prevent the prevalence of the bent-core properties such as anomalous elasticity, due to the lack of strong core-core interactions.

We note that the presence of alkyl chains on the arms of the molecules can also affect the anchoring strength. In future studies this also could be investigated, for example, using the method worked out by Sugiyama *et al.* [50].

VI. SUMMARY

We have studied the magnetic twist-Fréedericksz transition in the presence of pretilt with numerical modeling. We showed, that the nonzero director pretilt offers a dielectric measurement method to obtain the K_{22} elastic constant. We have simulated the light propagation through the cell and determined the transmittance as a function of magnetic inductance with different thickness and pretilt values. It was found that higher pretilt can qualitatively change the the transmittance profile. This is in contrast to the monotonic increase expected in the zero pretilt case near the threshold, where the major effect originates only from the depolarization effect. It was proven that the Mauguin effect causes trouble only in case of thick cells; with the thickness around 10 μm, the depolarization technique shows well the threshold values.

We have performed Fréedericksz-transition experiments in the splay and twist geometries to determine all the elastic constants of the BCN compound DT6PY6E6, using only a single planar cell. In the twist geometry, our theoretical considerations were confirmed by the measurements. We were able to determine K_{22} with the help of the dielectric method, which seems to be more versatile in many aspects than the conventional optical technique.

The elastic constants of DT6PY6E6 are found to be similar to that of rodlike materials. This is explained by the effect

of intermediate alkyl chains, which could prevent strong core-core interactions between molecules and increase the intermolecular distance.

ACKNOWLEDGMENTS

The authors are grateful to J. Kolacz for useful discussions on the numerical calculations. Financial support by the Hungarian Research Funds OTKA-K81250 and the NSF Grant No. DMR-0964765 are gratefully acknowledged.

APPENDIX

A monochromatic ray of light propagating along the z direction can be described by the x and y components of its electric field vector $E_x(z,t) = E_{0x}\cos(\omega t - kz)$, $E_y(z,t) = E_{0y}\cos(\omega t - kz + \delta)$, respectively [45]. ($\omega$, k, and δ are the angular frequency, the wave number, and the phase difference, respectively.) The **s** Stokes vector is constructed as

$$\mathbf{s} = \begin{bmatrix} s_0 \\ s_1 \\ s_2 \\ s_3 \end{bmatrix} = \begin{bmatrix} E_{0x}^2 + E_{0y}^2 \\ E_{0x}^2 - E_{0y}^2 \\ 2E_{0x}E_{0y}\cos\delta \\ 2E_{0x}E_{0y}\sin\delta \end{bmatrix}. \tag{A1}$$

For example, the Stokes vector for linearly polarized light in the x direction with the total intensity 1 is described by: $s_0 = 1$, $s_1 = 1$, $s_2 = 0$, and $s_3 = 0$.

The Mueller matrix of a birefringent slab with an optical phase difference of $\Delta\varphi$ is given by

$$\mathbf{M}_{wp}(\phi,\Delta\varphi) = \begin{bmatrix} 1 & 0 & 0 & 0 \\ 0 & \cos^2 2\phi + \cos\Delta\varphi \sin^2 2\phi & (1-\cos\Delta\varphi)\sin 2\phi\cos 2\phi & \sin\Delta\varphi\sin 2\phi \\ 0 & (1-\cos\Delta\varphi)\sin 2\phi\cos 2\phi & \sin^2 2\phi + \cos\Delta\varphi\sin^2 2\phi & -\sin\Delta\varphi\cos 2\phi \\ 0 & -\sin\Delta\varphi\sin 2\phi & \sin\Delta\varphi\cos 2\phi & \cos\Delta\varphi \end{bmatrix} \tag{A2}$$

ϕ is the angle between the slow axis and the x direction in our geometry.

The Mueller matrix of a polarizer set in an angle of α with respect to the x direction in our geometry

$$\mathbf{M}_{\mathrm{pol}}(\alpha) = \begin{bmatrix} 1 & \cos 2\alpha & \sin 2\alpha & 0 \\ \cos 2\alpha & \cos^2 2\alpha & \sin 2\alpha\cos 2\alpha & 0 \\ \sin 2\alpha & \sin 2\alpha\cos 2\alpha & \sin^2 2\alpha & 0 \\ 0 & 0 & 0 & 0 \end{bmatrix}. \tag{A3}$$

[1] P. G. de Gennes and J. Prost, *The Physics of Liquid Crystals*, 2nd ed. (Clarendon Press, Oxford, 1993).

[2] R. Stannarius, in *Handbook of Liquid Crystals*, Vol. 2A, edited by P. D. Demus, P. J. Goodby, P. G. W. Gray, P. H. W. Spiess, D. V. Vill, J. W. Goodby, and G. W. Gray (Wiley-VCH, Weinheim, 1998) Chap. III, pp. 60–90.

[3] M. Majumdar, P. Salamon, A. Jákli, J. T. Gleeson, and S. Sprunt, Phys. Rev. E **83**, 031701 (2011).

[4] P. P. Karat and N. V. Madhusudana, Mol. Cryst. Liq. Cryst. **40**, 239 (1976).

[5] H. P. Schad and M. A. Osman, J. Chem. Phys. **75**, 880 (1981).

[6] W. H. de Jeu, W. A. P. Claassen, and A. M. J. Spruijt, Mol. Cryst. Liq. Cryst. **37**, 269 (1976).

[7] W. H. de Jeu and W. A. P. Claassen, J. Chem. Phys. **67**, 3705 (1977).

[8] M. Schadt and F. Muller, IEEE Trans. Electron Devices **25**, 1125 (1978).

[9] F. Leenhouts and A. J. Dekker, J. Chem. Phys. **74**, 1956 (1981).

[10] P. A. Breddels and J. C. H. Mulkens, Mol. Cryst. Liq. Cryst. **147**, 107 (1987).

[11] L. A. Parry-Jones and M. A. Geday, Mol. Cryst. Liq. Cryst. **436**, 1213 (2005).

[12] F. Yang, J. R. Sambles, and G. W. Bradberry, J. Appl. Phys. **85**, 728 (1999).

[13] H. Hakemi, E. F. Jagodzinski, and D. B. Dupre, J. Chem. Phys. **78**, 1513 (1983).

[14] H. J. Coles and M. S. Sefton, Mol. Cryst. Liq. Cryst. **1**, 151 (1985).

[15] M. Hara, J. I. Hirakata, T. Toyooka, H. Takezoe, and A. Fukuda, Mol. Cryst. Liq. Cryst. **122**, 161 (1985).

[16] F. M. Leslie and C. M. Waters, Mol. Cryst. Liq. Cryst. **123**, 101 (1985).

[17] H. Takezoe, T. Toyooka, J. Hirakata, and A. Fukuda, Jpn. J. Appl. Phys., Part 2 **26**, L240 (1987).

[18] T. Toyooka, G. Chen, H. Takezoe, and A. Fukuda, Jpn. J. Appl. Phys., Part 1 **26**, 1959 (1987).

[19] G. P. Chen, H. Takezoe, and A. Fukuda, Liq. Cryst. **5**, 341 (1989).

[20] Z. Li, J. Appl. Phys. **75**, 1225 (1994).

[21] K. Ikeda, H. Okada, H. Onnagawa, and S. Sugimori, J. Appl. Phys. **86**, 5413 (1999).

[22] A. V. Dubtsov, S. V. Pasechnik, D. V. Shmeliova, V. A. Tsvetkov, and V. G. Chigrinov, Appl. Phys. Lett. **94**, 181910 (2009).

[23] J. Kezdzierski, Z. Raszewski, E. Nowinowski-Kruszelnicki, M. A. Kojdecki, W. Piecek, P. Perkowski, and E. Miszczyk, Mol. Cryst. Liq. Cryst. **544**, 57 (2011).

[24] J. Parka, M. Dabrowski, and R. Kowerdziej, Opto-Electron. Rev. **19**, 114 (2011).

[25] J. F. Stromer, C. V. Brown, and E. P. Raynes, Mol. Cryst. Liq. Cryst. **409**, 293 (2004).
[26] E. P. Raynes, C. V. Brown, and J. F. Stromer, Appl. Phys. Lett. **82**, 13 (2003).
[27] P. D. Brimicombe, C. Kischka, S. J. Elston, and E. P. Raynes, J. Appl. Phys. **101**, 043108 (2007).
[28] S. Faetti, M. Gatti, and V. Palleschi, J. Phys. Lett. (Paris) **46**, 881 (1985).
[29] H. Takezoe and Y. Takanishi, Jpn. J. Appl. Phys. **45**, 597 (2006).
[30] P. Salamon, N. Éber, A. Buka, J. T. Gleeson, S. Sprunt, and A. Jákli, Phys. Rev. E **81**, 031711 (2010).
[31] J. Harden, B. Mbanga, N. Éber, K. Fodor-Csorba, S. Sprunt, J. T. Gleeson, and A. Jákli, Phys. Rev. Lett. **97**, 157802 (2006).
[32] P. S. Salter, C. Tschierske, S. J. Elston, and E. P. Raynes, Phys. Rev. E **84**, 031708 (2011).
[33] S. Kaur, A. Belaissaoui, J. W. Goodby, V. Görtz, and H. F. Gleeson, Phys. Rev. E **83**, 041704 (2011).
[34] P. Tadapatri, U. S. Hiremath, C. V. Yelamaggad, and K. S. Krishnamurthy, J. Phys. Chem. B **114**, 10 (2010).
[35] P. Tadapatri, K. S. Krishnamurthy, and W. Weissflog, Phys. Rev. E **82**, 031706 (2010).
[36] S. Tanaka, H. Takezoe, N. Éber, K. Fodor-Csorba, A. Vajda, and A. Buka, Phys. Rev. E **80**, 021702 (2009).
[37] D. Wiant, J. T. Gleeson, N. Éber, K. Fodor-Csorba, A. Jákli, and T. Tóth-Katona, Phys. Rev. E **72**, 041712 (2005).
[38] O. Francescangeli, V. Stanic, S. I. Torgova, A. Strigazzi, N. Scaramuzza, C. Ferrero, I. P. Dolbnya, T. M. Weiss, R. Berardi, L. Muccioli, S. Orlandi, and C. Zannoni, Adv. Funct. Mater. **19**, 2592 (2009).
[39] O. Francescangeli, F. Vita, C. Ferrero, T. Dingemans, and E. T. Samulski, Soft Matter **7**, 895 (2011).
[40] S. H. Hong, R. Verduzco, J. T. Gleeson, S. Sprunt, and A. Jákli, Phys. Rev. E **83**, 061702 (2011).
[41] P. Sathyanarayana, M. Mathew, Q. Li, V. S. S. Sastry, B. Kundu, K. V. Le, H. Takezoe, and S. Dhara, Phys. Rev. E **81**, 010702 (2010).
[42] P. Sathyanarayana, B. K. Sadashiva, and S. Dhara, Soft Matter **7**, 8556 (2011).
[43] P. Tadapatri, U. S. Hiremath, C. Yelamaggad, and K. Krishnamurthy, J. Phys. Chem. B **114**, 1745 (2010).
[44] E. Hecht, *Optics*, 4th ed. (Addison Wesley, San Francisco, 2002).
[45] E. Collett, *Field Guide to Polarization* (SPIE, Washington, 2005).
[46] D.-K. Yang and S.-T. Wu, *Fundamentals of Liquid Crystal Devices* (Wiley, Chichester, 2006).
[47] J. Seltmann, A. Marini, B. Mennucci, S. Dey, S. Kumar, and M. Lehmann, Chem. Mater. **23**, 2630 (2011).
[48] B. R. Ratna, R. Shashidhar, Pramana **6**, 278 (1976).
[49] A. Buka and W. H. de Jeu, J. Phys. (Paris) **43**, 361 (1982).
[50] T. Sugiyama, S. Kuniyasu, D. Seo, H. Fukuro, and S. Kobayashi, Jpn. J. Appl. Phys., Part 1 **29**, 2045 (1990).